

R. Partridge³², N. Parua¹⁴, A. Patwa¹⁴, O. Peters¹⁹, P. Pétrouff³, R. Piegaia⁴⁷, B. G. Pope⁴, H. B. Prosper²⁵, S. Protopopescu⁷, M. B. Przybycien^{33*}, J. Qian¹⁰, S. Rajagopalan⁷, P. A. Rapidis¹⁸, N. W. Reay²⁹, S. Reucroft²⁰, M. Ridel³, M. Rijssenbeek¹⁴, F. Rizatdinova²⁹, T. Rockwell⁴, C. Royon⁴¹, P. Rubinov¹⁸, R. Ruchti⁴⁵, B. M. Sabirov¹, G. Sajot¹², A. Santoro³⁶, L. Sawyer⁴⁶, R. D. Schamberger¹⁴, H. Schellman³³, A. Schwartzman⁴⁷, E. Shabalina⁸, R. K. Shivpuri⁵⁸, D. Shpakov²⁰, M. Shupe⁵³, R. A. Sidwell²⁹, V. Simak⁵⁵, V. Sirotenko¹⁸, P. Slattery²⁴, R. P. Smith¹⁸, G. R. Snow³⁹, J. Snow⁵⁷, S. Snyder⁷, J. Solomon⁸, Y. Song³¹, V. Sorin⁴⁷, M. Sosebee³¹, N. Sotnikova⁴², K. Soustruznik⁵⁴, M. Souza¹¹, N. R. Stanton²⁹, G. Steinbrück³⁰, D. Stoker⁵⁹, V. Stolin⁴⁴, A. Stone⁸, D. A. Stoyanova⁵, M. A. Strang³¹, M. Strauss², M. Strovink⁴⁰, L. Stutte¹⁸, A. Sznajder³⁶, M. Talby¹⁷, W. Taylor¹⁴, S. Tentiendo-Repond²⁵, T. G. Trippe⁴⁰, A. S. Turcot⁷, P. M. Tuts³⁰, R. Van Kooten²³, V. Vaniev⁵, N. Varelas⁸, F. Villeneuve-Seguier¹⁷, A. A. Volkov⁵, A. P. Vorobiev⁵, H. D. Wahl²⁵, Z.-M. Wang¹⁴, J. Warchol⁴⁵, G. Watts⁶⁰, M. Wayne⁴⁵, H. Weerts⁴, A. White³¹, D. Whiteson⁴⁰, D. A. Wijngaarden⁹, S. Willis²⁸, S. J. Wimpenny³⁸, J. Womersley¹⁸, D. R. Wood²⁰, Q. Xu¹⁰, R. Yamada¹⁸, T. Yasuda¹⁸, Y. A. Yatsunenkov¹, K. Yip⁷, J. Yu³¹, M. Zanabria¹³, X. Zhang², B. Zhou¹⁰, Z. Zhou⁵⁰, M. Zielinski²⁴, D. Zieminska²³, A. Ziemiński²³, V. Zutshi²⁸, E. G. Zverev⁴² & A. Zylberstein⁴¹

Affiliations for participants: 1, Joint Institute for Nuclear Research, P O Box 79, 141980 Dubna, Russia; 2, University of Oklahoma, Department of Physics and Astronomy, Norman, Oklahoma 73019, USA; 3, Laboratoire de l'Accélérateur Linéaire, IN2P3-CNRS, BP 34, Batiment 200, F-91898 Orsay, France; 4, Michigan State University, Department of Physics and Astronomy, East Lansing, Michigan 48824, USA; 5, Institute for High Energy Physics, 142284 Protvino, Russia; 6, Tata Institute of Fundamental Research, School of Natural Sciences, Homi Bhabha Rd, Mumbai 400005, India; 7, Brookhaven National Laboratory, Physics Department, Bldg 510C, Upton, New York 11973, USA; 8, University of Illinois at Chicago, Department of Physics, 845 W. Taylor, Chicago, Illinois 60607, USA; 9, University of Nijmegen/NIKHEF, P O Box 9010, NL-6500 GL Nijmegen, The Netherlands; 10, University of Michigan, Department of Physics, 500 E. University Avenue, Ann Arbor, Michigan 48109, USA; 11, LAFEX, Centro Brasileiro de Pesquisas Físicas, Rua Dr Xavier Sigaud, 150, 22290-180 Rio de Janeiro, Brazil; 12, Laboratoire de Physique Subatomique et de Cosmologie, IN2P3-CNRS, Université de Grenoble 1, 53 Avenue des Martyrs, F-38026 Grenoble, France; 13, Universidad de los Andes, Department de Física, HEP Group, Apartado Aereo 4976, Bogotá, Colombia; 14, State University of New York, Department of Physics and Astronomy, Stony Brook, New York 11794, USA; 15, Imperial College London, Department of Physics, Prince Consort Road, London SW7 2BW, UK; 16, University of Maryland, Department of Physics, College Park, Maryland 20742, USA; 17, CPPM, IN2P3-CNRS, Université de la Méditerranée, 163 Avenue de Luminy, F-13288 Marseille, France; 18, Fermi National Accelerator Laboratory, P O Box 500, Batavia, Illinois 60510, USA; 19, FOM-Institute NIKHEF and University of Amsterdam/NIKHEF, P O Box 41882, 1009 DB Amsterdam, The Netherlands; 20, Northeastern University, Department of Physics, Boston, Massachusetts 02115, USA; 21, University of Kansas, Department of Physics and Astronomy, 1251 Wescoe Hall Drive, Lawrence, Kansas 66045, USA; 22, LPNHE, Universités Paris VI and VII, IN2P3-CNRS, 4 Place Jussieu, Tour 33, F-75252 Paris, France; 23, Indiana University, Department of Physics, 727 E. 3rd St, Bloomington, Indiana 47405, USA; 24, University of Rochester, Department of Physics and Astronomy, Rochester, New York 14627, USA; 25, Florida State University, Department of Physics 4350, Tallahassee, Florida 32306, USA; 26, Panjab University, Department of Physics, Chandigarh 160014, India; 27, Lancaster University, Department of Physics, Lancaster LA1 4YB, United Kingdom; 28, Northern Illinois University, Department of Physics, DeKalb, Illinois 60115, USA; 29, Kansas State University, Department of Physics, Manhattan, Kansas 66506, USA; 30, Columbia University, Department of Physics, 538 W. 120th St, New York, New York 10027, USA; 31, University of Texas, Department of Physics, Box 19059, Arlington, Texas 76019, USA; 32, Brown University, Department of Physics, 182 Hope St, Providence, Rhode Island 02912, USA; 33, Northwestern University, Department of Physics and Astronomy, 2145 Sheridan Road, Evanston, Illinois 60208, USA; 34, Universität Freiburg, Physikalisches Institut, Hermann-Herder-Strasse 3, 79104 Freiburg, Germany; 35, Boston University, Department of Physics, 590 Commonwealth Avenue, Boston, Massachusetts 02215, USA; 36, Universidade do Estado do Rio de Janeiro, Instituto de Física, Rua São Francisco Xavier, 524, 20559-900 Rio de Janeiro, Brazil; 37, CINVESTAV, Departamento de Física, P O Box 14-740, 07000 Mexico City, Mexico; 38, University of California, Department of Physics, Riverside, California 92521, USA; 39, University of Nebraska, Department of Physics and Astronomy, Lincoln, Nebraska 68588, USA; 40, Lawrence Berkeley National Laboratory and University of California, 1 Cyclotron Road, Berkeley, California 94720, USA; 41, DAPNIA/Service de Physique des Particules, CEA, Saclay, F-91191 Gif-sur-Yvette, France; 42, Moscow State University, Department of Physics, Vorobjovoy Gory, 119899 Moscow, Russia; 43, Rice University, Bonner Nuclear Lab, P O Box 1892, Houston, Texas 77005, USA; 44, Institute for Theoretical and Experimental Physics, B. Chermushkinskaya ul. 25, 117259 Moscow, Russia; 45, University of Notre Dame, Department of Physics, Notre Dame, Indiana 46556, USA; 46, Louisiana Tech University, Department of Physics, Ruston, Louisiana 71272, USA; 47, Universidad de Buenos Aires, Departamento de Física, FCEN, Pabellón 1, Ciudad Universitaria, 1428 Buenos Aires, Argentina; 48, University College Dublin, Department of Experimental Physics, Faculty of Science, Belfield, Dublin 4, Ireland; 49, California State University, Department of Physics, 2345 E. San Ramon Avenue, Fresno, California 93740, USA; 50, Iowa State University, Department of Physics, High Energy Physics Group, Ames, Iowa 50011, USA; 51, University of Virginia, Department of Physics, Charlottesville, Virginia 22901, USA; 52, Universidad San Francisco de Quito, P O Box 17-12-841, Quito, Ecuador; 53, University of Arizona, Department of Physics, P O Box 210081, Tucson, Arizona 85721, USA; 54, Institute of Particle and Nuclear Physics, Center for Particle Physics, Faculty of Mathematics and Physics, Charles University in Prague, V Holesovickach 2, CZ-18000 Prague 8, Czech Republic; 55, Institute of Physics of the Academy of Sciences of the Czech Republic, Center for Particle Physics, Na Slovance 2, CZ-18221 Prague 8, Czech Republic; 56, Institute of High Energy Physics, P O Box 918, Beijing 100039, China; 57, Langston University, Department of Mathematics, Langston, Oklahoma 73050, USA; 58, Delhi University, Department of Physics and Astrophysics, Delhi 110007, India; 59, University of California, Department of Physics and Astronomy, 4129 Frederick Reines Hall, Irvine, California 92697, USA; 60, University of Washington, Department of Physics, P O Box 351560, Seattle, Washington 98195, USA.

*Present addresses: University of Zurich, Zurich, Switzerland (E.L.); Institute of Nuclear Physics, Krakow, Poland (M.B.P.)

Energy-transfer pumping of semiconductor nanocrystals using an epitaxial quantum well

Marc Achermann¹, Melissa A. Petruska¹, Simon Kos¹, Darryl L. Smith¹, Daniel D. Koleske² & Victor I. Klimov¹

¹Los Alamos National Laboratory, Los Alamos, New Mexico 87545, USA

²Sandia National Laboratories, Albuquerque, New Mexico 87185, USA

As a result of quantum-confinement effects, the emission colour of semiconductor nanocrystals can be modified dramatically by simply changing their size^{1,2}. Such spectral tunability, together with large photoluminescence quantum yields and high photostability, make nanocrystals attractive for use in a variety of

light-emitting technologies—for example, displays, fluorescence tagging³, solid-state lighting and lasers⁴. An important limitation for such applications, however, is the difficulty of achieving electrical pumping, largely due to the presence of an insulating organic capping layer on the nanocrystals. Here, we describe an approach for indirect injection of electron–hole pairs (the electron–hole radiative recombination gives rise to light emission) into nanocrystals by non-contact, non-radiative energy transfer from a proximal quantum well that can in principle be pumped either electrically or optically. Our theoretical and experimental results indicate that this transfer is fast enough to compete with electron–hole recombination in the quantum well, and results in greater than 50 per cent energy-transfer efficiencies in the tested structures. Furthermore, the measured energy-transfer rates are sufficiently large to provide pumping in the stimulated emission regime, indicating the feasibility of nanocrystal-based optical amplifiers and lasers based on this approach.

Several programs worldwide (for example, ref. 5) emphasize the need for efficient solid-state emitters in applications ranging from displays and traffic signs to solid-state lighting. Semiconductor nanocrystals are considered to be promising nanoscale colour-selectable emitters that combine high (potentially 100%) photoluminescence quantum yields with chemical flexibility and processibility. Even in the form of a single monolayer they can produce significant power outputs of the order of watts per cm^2 (estimated for a nanocrystal packing density of 10^{12} cm^{-2} , a radiative lifetime of 20 ns, and a moderate quantum yield of 20%).

One approach to nanocrystal-based, electrically pumped light-emitting devices uses hybrid organic/inorganic structures, in which the charges are delivered to nanocrystals through the organic network and/or percolated nanocrystal subsystem^{6–8}. The performance of these devices is, however, limited by low carrier mobilities in both the organic and nanocrystal components, and by the poor stability of organic molecules with respect to photooxidation. Here, we explore a novel, ‘non-contact’ approach to carrier injection into nanocrystals using Förster-like non-radiative energy transfer from a proximal epitaxial quantum well. As energy transfer relies on Coulomb interactions rather than a direct wavefunction overlap, it is not significantly inhibited by the nanocrystal capping layer, and it can potentially allow for an efficient energy flow from a quantum well to nanocrystals. In a real-life device, the quantum well can be pumped electrically in the same way a common quantum-well light-emitting diode is pumped. However, in this work we intentionally

use pulsed optical excitation to study the dynamics of energy transfer as well as the dynamics of other competing processes such as carrier recombination in the quantum well.

The structure studied in our experiments is depicted in Fig. 1a. It consists of an InGaN quantum well, on top of which is assembled a close-packed monolayer of highly monodisperse CdSe/ZnS core/shell nanocrystals using the Langmuir–Blodgett technique. The nanocrystals were synthesized as described in refs 2 and 9 and consist of a CdSe core (radius = 1.9 nm) overcoated with a shell of ZnS (~0.6 nm thickness), followed by a final layer of the organic molecules trioctylphosphine (TOP) and trioctylphosphine oxide (TOPO). These nanocrystals show efficient emission centred near 575 nm and a structured absorption spectrum with the lowest 1S absorption maximum at ~560 nm (Fig. 1b). Quantum-well samples were grown on sapphire substrates by metal–organic chemical-vapour deposition¹⁰. They consisted of a 20-nm GaN nucleation layer, a 3- μm GaN bottom barrier, and a 3-nm InGaN quantum well that was either terminated with a 3-nm GaN top barrier (capped quantum well) or remained uncapped. The concentration of In in the quantum wells was 5–10%, which corresponds to an emission wavelength of ~400 nm (Fig. 1b). This wavelength is in the range of strong nanocrystal absorption, which provides strong coupling of quantum-well excitations to the absorption dipole of nanocrystals, and should allow efficient energy transfer. To study energy-transfer dynamics, we monitored the temporal evolution of photoluminescence in the quantum well and the nanocrystals using a time-correlated single-photon counting system that provides ~30 ps time resolution. The hybrid quantum-well/nanocrystal structures were excited at 266 nm by 200-fs pulses of the frequency-tripled output of an amplified Ti:sapphire laser. The emission from either the quantum well or the nanocrystals was selected using a monochromator. The dynamics measured for quantum-well/nanocrystal hybrid structures were compared with those in isolated quantum wells and isolated nanocrystal monolayers assembled on glass substrates. All measurements were performed at room temperature.

The interactions between the quantum well and the nanocrystal monolayer can be described in terms of a resonant Förster-type energy transfer¹¹. The energy-transfer rate per quantum-well carrier is strongly dependent on whether electrons and holes are free or bound by Coulomb interactions into excitons. In the case of excitons, the energy-transfer rate is independent of the density of quantum-well excitations (n_{eh}), whereas in the free-carrier case, the energy-transfer rate is proportional to n_{eh} (see Supplementary Information). To distinguish experimentally between these two cases, we measured the excitation-density dependence of photoluminescence in an isolated quantum well at $t = 0$ ps (Fig. 2). We observe that at low pump powers this dependence is quadratic, and it saturates at high excitation densities. The quadratic growth of photoluminescence is characteristic of free-carrier bimolecular recombination, indicating that electron–hole interactions in our quantum-well samples are not sufficiently strong to produce bound exciton states at room temperature. We also monitor the photoluminescence dynamics in the quantum well (Fig. 2b) and observe that the photoluminescence decay is exponential and is characterized by a time constant range of 0.6–1 ns that is independent of pump power. This result indicates that the decay of photoexcited carriers is dominated not by radiative recombination (characterized by the density-dependent time constant $\tau \propto 1/n_{eh}$) but by trapping at defects, as is typically observed for InGaN quantum wells at room temperature.

After establishing that quantum-well excitations are unbound electron–hole pairs, we can analyse the energy-transfer rate, Γ_{ET} per quantum-well carrier using the following expression (see

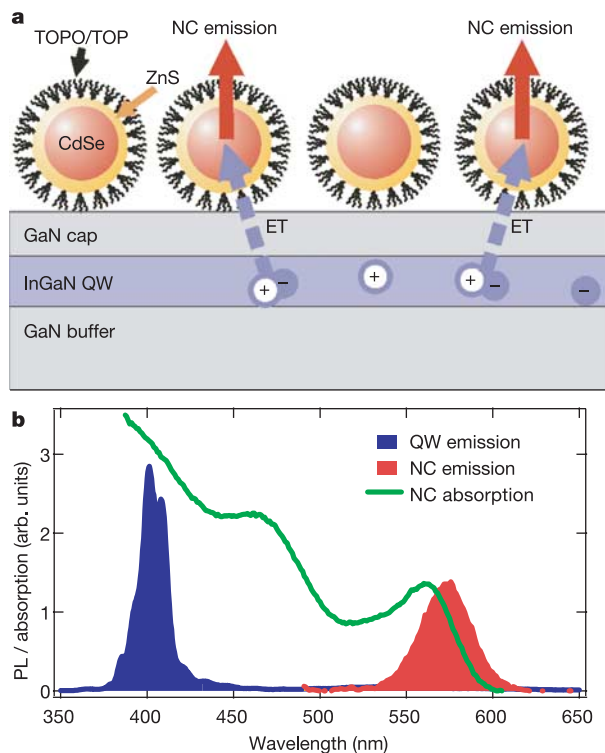


Figure 1 Schematic and optical properties of the hybrid quantum-well/nanocrystal structure. **a**, The structure consists of an InGaN/GaN quantum-well heterostructure with a monolayer of TOPO/TOP-capped CdSe/ZnS core/shell nanocrystals on top of it. Electron–hole pairs generated in the quantum well can experience non-radiative resonant transfer into nanocrystals by Förster-type, dipole–dipole interactions. The nanocrystals excited by energy transfer produce emission with a wavelength determined by the nanocrystal size. **b**, The emission of the quantum well (blue) spectrally overlaps with the absorption of the nanocrystals (green). For CdSe nanocrystals with 1.9 nm radius, the emission wavelength is around 575 nm (red). PL is photoluminescence.

Supplementary Information):

$$\Gamma_{ET} = \frac{8\pi^2}{3\epsilon^2} |\mu_{NC}|^2 |\mu_{QW}|^2 n_{NC} n_{eh} N_{NC}(\hbar\omega_{QW}) \times \frac{1}{d^4} \frac{\hbar^2}{2Mk_B T} \int_0^\infty \kappa^3 \exp\left(-2\kappa - \frac{\hbar^2 \kappa^2}{2Mk_B T d^2}\right) d\kappa \quad (1)$$

in which ϵ is the dielectric constant, μ_{NC} and μ_{QW} are the transition dipole moments for the nanocrystal and the quantum well, respectively, n_{NC} is the surface density of nanocrystals, $N_{NC}(\hbar\omega_{QW})$ is the nanocrystal density of states at the quantum-well emission energy $\hbar\omega_{QW}$, d is the separation between the centres of the quantum well and the nanocrystal monolayer, M is the sum of electron and hole masses in the quantum well, T is the temperature, κ is the in-plane centre-of-mass momentum of the electron-hole pair in the quantum well in units of \hbar/d , and k_B is the Boltzmann constant. Assuming that the length of nanocrystal-passivating molecules is 1.1 nm, we find that d is 8.1 and 5.1 nm for capped and uncapped quantum wells, respectively, which further results in transfer rates of 1.05 ns^{-1} (capped quantum well) and 5.8 ns^{-1} (uncapped quantum well) at a quantum-well carrier density of $1.8 \times 10^{13} \text{ cm}^{-2}$. These estimated energy-transfer rates are sufficiently high to compete with carrier-decay rates ($\sim 1 \text{ ns}^{-1}$) measured experimentally for our quantum-well samples.

To measure directly the quantum-well-to-nanocrystal (QW-NC) energy-transfer rates, we perform comparative, time-resolved

photoluminescence studies for hybrid quantum-well/nanocrystal structures and isolated quantum wells. We observe that the presence of the nanocrystal layer adjacent to the quantum well significantly alters the quantum-well photoluminescence dynamics (Fig. 3a). Namely, the quantum-well photoluminescence decay becomes faster in the presence of nanocrystals, indicating an additional relaxation channel for quantum-well excitations, which is most likely due to QW-NC energy transfer (see the analysis below). This nanocrystal-induced change in quantum-well dynamics becomes more pronounced with increasing carrier density (compare traces shown by solid and dashed lines in Fig. 3a). To quantify this increase, in Fig. 3b we plot the additional initial decay rate $\Delta\Gamma = \Gamma_{QW \text{ with NC}} - \Gamma_{QW \text{ without NC}}$ as a function of n_{eh} for structures based on uncapped and capped quantum wells. We observe that in both cases the $\Delta\Gamma$ growth is linear with n_{eh} , but absolute values of $\Delta\Gamma$ are approximately 4.4 times greater for the uncapped quantum wells compared with quantum wells with a top barrier. Both of these observations are consistent with the fact that the additional decay rate $\Delta\Gamma$ is due to QW-NC energy transfer. Förster modelling (equation (1)) predicts that for the free-carrier case, the energy-transfer rate should increase linearly with n_{eh} , which is exactly the dependence observed experimentally. Furthermore, the increase in the transfer rate in the case of the uncapped quantum well is consistent with its strong dependence on the energy-transfer distance ($\Gamma_{ET} \sim d^{-4}$). From the geometrical parameters of our system, we estimate that the d dependence should result in a 5.5

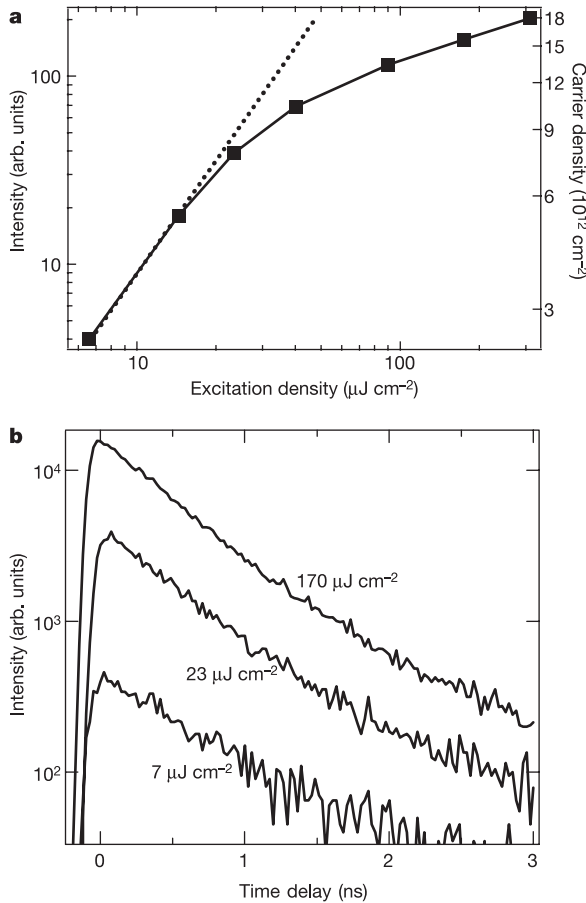


Figure 2 Pump- and time-dependent emission from an isolated quantum well. **a**, The photoluminescence intensity of the quantum well (squares) at zero time delay is plotted as a function of pump fluence. The dotted line is a fit to the quadratic growth at low pump fluences. **b**, Photoluminescence dynamics of the isolated quantum well measured at different pump fluences.

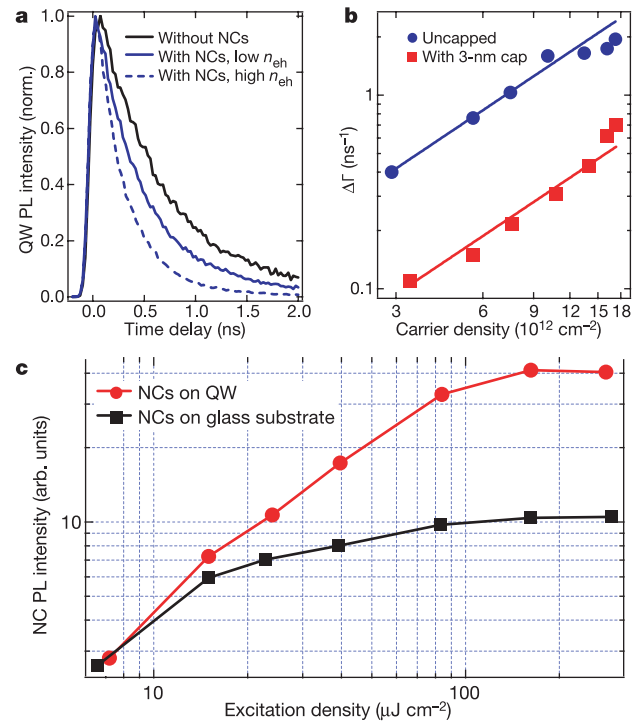


Figure 3 Experimental observations of QW-NC energy transfer. **a**, Normalized photoluminescence dynamics of the isolated quantum well (black solid line) at $n_{eh} = 3 \times 10^{12} \text{ cm}^{-2}$ in comparison with quantum-well photoluminescence dynamics measured for the quantum-well/nanocrystal structure at $n_{eh} = 3 \times 10^{12} \text{ cm}^{-2}$ (blue solid line) and $n_{eh} = 10 \times 10^{12} \text{ cm}^{-2}$ (blue dashed line). **b**, The difference between the initial photoluminescence decay rates measured for the isolated quantum well and the quantum-well/nanocrystal structure ($\Delta\Gamma = \Gamma_{QW \text{ with NC}} - \Gamma_{QW \text{ without NC}}$) versus quantum-well carrier density for samples based on the capped and the uncapped quantum well. **c**, Time-integrated nanocrystal photoluminescence intensity versus pump fluence for the nanocrystal monolayer assembled on a glass substrate and on top of a capped quantum well.

increased energy-transfer rate, which agrees well with the factor of 4.4 observed experimentally.

Further evidence for efficient QW–NC energy-transfer is provided by the analysis of the photoluminescence from the nanocrystal layer. The energy-transfer-induced outflow of carriers from the quantum well should result in a corresponding increase in the emission of the nanocrystals. In our experimental configuration, however, optical pumping directly generates carriers not only in the quantum well but also in the nanocrystals. Therefore, to extract the energy-transfer-induced increase in the nanocrystal photoluminescence, we perform a side-by-side comparison of photoluminescence data for hybrid quantum-well/nanocrystal structures and a nanocrystal Langmuir–Blodgett monolayer assembled on a glass slide. One such set of data plotted as temporally integrated nanocrystal photoluminescence intensity versus pump fluence is displayed in Fig. 3c. To account for the difference in the nanocrystal packing densities for

Langmuir–Blodgett films assembled on the quantum well and the glass slide, we introduce a constant scaling factor, which allows us to match photoluminescence intensities detected from quantum-well/nanocrystal and glass/nanocrystal samples at low pump powers, for which energy transfer from the quantum well is negligible. The data indicate that at low pump fluences, both types of samples show a similar photoluminescence pump dependence. However, two traces show distinctly different behaviour at higher pump fluences, for which energy transfer starts to play a significant role (Fig. 3b). Whereas emission from the isolated nanocrystal layer saturates at $\sim 20 \mu\text{J cm}^{-2}$, the nanocrystal photoluminescence in the hybrid structure shows a steady growth until $\sim 80 \mu\text{J cm}^{-2}$. As a result of this delayed saturation, the maximum nanocrystal photoluminescence intensity achievable with the quantum-well/nanocrystal structure is four times greater than the photoluminescence for the nanocrystal monolayer on the glass slide. All of these results indicate a strong additional carrier inflow into nanocrystals as a result of energy transfer from the quantum well.

Figure 4a displays the schematics of energy transfer along with other relaxation processes in the hybrid quantum-well/nanocrystal structures studied in this work. Following photoexcitation, carrier thermalization, and cooling, the thermal distribution of free electrons and holes is established in the quantum well. Quantum-well carriers can decay either radiatively (time constant τ_{rr}) or non-radiatively (τ_{nr}), or experience energy transfer (τ_{ET}) into a nanocrystal. Carriers generated in the nanocrystal by resonant QW–NC energy transfer have significant excess energies as measured with respect to the nanocrystal bandgap. Extremely fast intraband relaxation in nanocrystals (subpicosecond time scales)^{12,13} rapidly removes carriers from resonance with the quantum-well transition and prevents backtransfer. In well-passivated nanocrystals, relaxed electron–hole pairs recombine primarily radiatively with a time constant of ~ 20 ns, emitting a photon with an energy that is determined by the nanocrystal size.

The efficiency of non-radiative QW–NC energy-transfer (η_{ET}) can be estimated from the expression: $\eta_{ET} = \tau_r (\tau_{ET} + \tau_r)^{-1}$, in which $\tau_r = (1/\tau_{rr} + 1/\tau_{nr})^{-1}$ is the relaxation time of quantum-well excitations due to both radiative and non-radiative process. Our experimental results for the uncapped sample indicate that $\tau_r \approx 0.6$ ns and $\tau_{ET} \approx 0.5$ ns (for $n_{eh} = 1.8 \times 10^{13} \text{ cm}^{-2}$), which yields η_{ET} as high as 55%. We believe that nearly 100% efficiencies can be achieved by improving the quality of the quantum wells (to reduce non-radiative losses) and/or by optimizing the geometry of the nanocrystal/quantum-well structure (by using, for example, shorter nanocrystal surface-passivation molecules).

It is interesting that despite the additional step in the energy-transfer process, the photoluminescence quantum yield of the hybrid quantum-well/nanocrystal device ($QY_{QW/NC}$) can be greater than the original quantum yield of the quantum well. $QY_{QW/NC}$ can be estimated from the expression $QY_{QW/NC} = QY_{NC} (1 + \tau_{ET}/\tau_r)^{-1}$. This expression indicates that if $\tau_{ET} \ll \tau_r$ the quantum efficiency of the hybrid structure approaches that of nanocrystals. This conclusion further means that even the use of InGaN quantum wells with poor room-temperature quantum yields can produce highly efficient hybrid devices.

It is illustrative to compare the efficiency of energy transfer measured here with that expected for radiative energy transfer (η_{RET}). The latter process is used in the traditional colour-conversion scheme, and is based on the emission of a photon from a quantum well followed by absorption/re-emission steps in the phosphor material (nanocrystals in our case). For a close-packed nanocrystal monolayer, η_{RET} can be estimated from the ratio of the nanocrystal absorption cross-section¹⁴ to its geometrical cross-section, which yields $\eta_{RET} < 0.3\%$. This value is at least two orders of magnitude smaller than the efficiencies measured experimentally, indicating that the use of non-radiative energy transfer

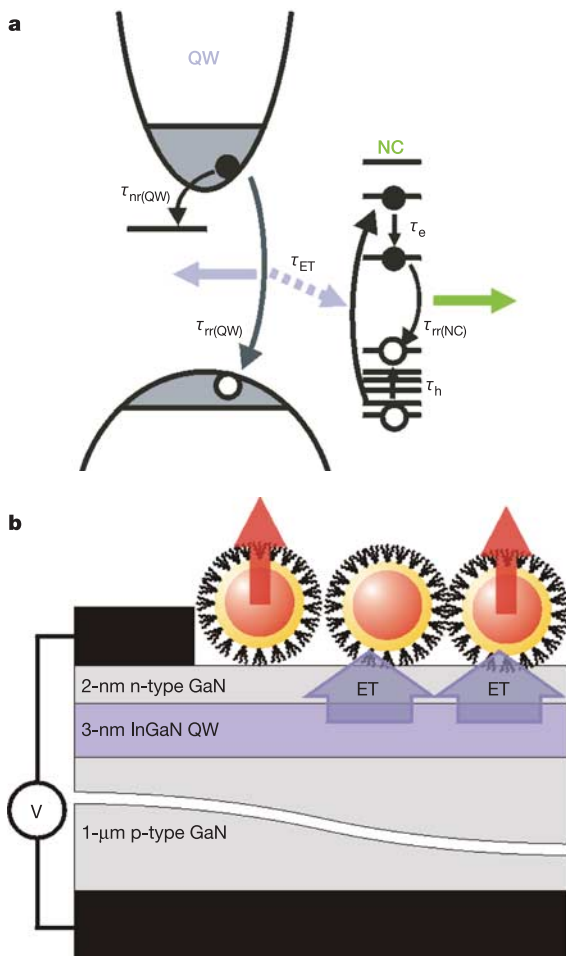


Figure 4 Carrier relaxation and energy-transfer processes in the hybrid quantum-well/nanocrystal structure and a schematic of an electrically driven energy-transfer device. **a**, The QW–NC energy transfer competes with radiative and non-radiative decay processes in the quantum well. High-energy excitations created in the nanocrystals through energy transfer rapidly relax (time constants τ_e and τ_h) to the nanocrystal band edge, which prevents backtransfer. Subscript e is electron and h is hole. **b**, An electrically powered hybrid quantum-well/nanocrystal device that can be used to realize the ‘energy-transfer colour-converter’ in the regime of electrical injection. It depicts an InGaN quantum well sandwiched between bottom p-type and thin, top n-type GaN barriers with attached metal contacts. The top contact only partially covers the quantum well and leaves open space for assembling the nanocrystals.

can significantly improve the performance of colour-conversion devices.

In addition to applications as efficient colour converters, nanocrystals have been considered promising building blocks for colour-selectable optical-gain media in lasing applications⁴. One complication associated with lasing applications of nanocrystals is the requirement for extremely fast pumping that competes with non-radiative Auger recombination, leading to very short (picosecond) optical gain lifetimes¹⁵. So far, optical amplification and lasing in nanocrystals has been achieved using optical excitation with short laser pulses. Our estimations show that the 'energy-transfer pumping' scheme studied here provides carrier inflow that can in principle compete with non-radiative losses induced by Auger recombination. The energy-transfer rate of $\sim 2 \text{ ns}^{-1}$ measured for the uncapped quantum-well sample for $n_{\text{ch}} = 1.8 \times 10^{13} \text{ cm}^{-2}$ results in a QW-NC carrier flux of $\sim 3.6 \times 10^{22} \text{ cm}^{-2} \text{ s}^{-1}$. For the nanocrystals of 1.9 nm radius studied here, the Auger recombination time is $\sim 50 \text{ ps}$, which corresponds to a non-radiative carrier loss of $4 \times 10^{22} \text{ cm}^{-2} \text{ s}^{-1}$ for a close-packed monolayer. The latter value is comparable to the carrier inflow rate provided by energy transfer from the quantum well, indicating the feasibility of lasing in the energy-transfer pumping regime.

Although in this report we have studied optically pumped devices, it should be possible to realize the energy-transfer pumping scheme in the regime of electrical injection by combining nanocrystals with an electrically driven InGaN quantum well. The design of the quantum-well emitter in the 'energy-transfer colour-converter' (Fig. 4b) can be similar to that used in conventional InGaN light-emitting diodes, in which the quantum well is sandwiched between n- and p-doped GaN barriers with attached metal contacts¹⁶. Our preliminary studies indicate that we can fabricate relatively high mobility, thin (2–3 nm), n-doped GaN layers that can be used as top quantum-well barriers (adjacent to nanocrystals) in electrically powered devices. The direct comparison of photoluminescence dynamics in nanocrystals assembled on glass slides and n-doped GaN layers (up to $2 \times 10^{19} \text{ cm}^{-3}$ doping level) do not show any noticeable quenching of nanocrystal emission in the presence of a proximal, doped semiconductor. Furthermore, the doping of the barriers is not expected to induce additional carrier losses in the quantum well^{17,18}. All of these considerations strongly indicate the feasibility of high-efficiency, electrically driven, hybrid nanocrystal/quantum-well devices. □

Received 9 February; accepted 19 April 2004; doi:10.1038/nature02571.

- Alivisatos, A. P. Semiconductor clusters, nanocrystals, and quantum dots. *Science* **271**, 933–937 (1996).
- Murray, C. B., Norris, D. J. & Bawendi, M. G. Synthesis and characterization of nearly monodisperse CdE (E = S, Se, Te) semiconductor nanocrystallites. *J. Am. Chem. Soc.* **115**, 8706–8715 (1993).
- Bruchez, M., Moronne, M., Gin, P., Weiss, S. & Alivisatos, A. P. Semiconductor nanocrystals as fluorescent biological labels. *Science* **281**, 2013–2016 (1998).
- Klimov, V. I. *et al.* Optical gain and stimulated emission in nanocrystal quantum dots. *Science* **290**, 314–317 (2000).
- Next-Generation Lighting Initiative* <http://lighting.sandia.gov/Xlightinginit.htm#snlngli>
- Colvin, V., Schlamp, M. & Alivisatos, A. Light-emitting diodes made from cadmium selenide nanocrystals and a semiconducting polymer. *Nature* **370**, 354–357 (1994).
- Schlamp, M. C., Peng, X. G. & Alivisatos, A. P. Improved efficiencies in light emitting diodes made with CdSe(CdS) core/shell type nanocrystals and a semiconducting polymer. *J. Appl. Phys.* **82**, 5837–5842 (1997).
- Coe, S., Woo, W.-K., Bawendi, M. & Bulovic, V. Electroluminescence from single monolayers of molecular organic devices. *Nature* **420**, 800–803 (2002).
- Dabbousi, B. O. *et al.* (CdSe)ZnS core-shell quantum dots: synthesis and characterization of a size series of highly luminescent nanocrystallites. *J. Phys. Chem.* **101**, 9463–9475 (1997).
- Koleske, D. D. *et al.* Improved brightness of 380 nm GaN light emitting diodes through intentional delay of the nucleation island coalescence. *Appl. Phys. Lett.* **81**, 1940–1942 (2002).
- Basko, D., La Rocca, G. C., Bassani, F. & Agranovich, V. M. Förster energy transfer from a semiconductor quantum well to an organic material overlayer. *Eur. Phys. J. B* **8**, 353–362 (1999).
- Klimov, V. I. & McBranch, D. W. Femtosecond IP-to-IS electron relaxation in strongly confined semiconductor nanocrystals. *Phys. Rev. Lett.* **80**, 4028–4031 (1998).
- Xu, S., Mikhailovsky, A. A., Hollingsworth, J. A. & Klimov, V. I. Hole intraband relaxation in strongly confined quantum dots: Revisiting the "phonon bottleneck" problem. *Phys. Rev. B* **65**, 045319 (2002).
- Klimov, V. I. Optical nonlinearities and ultrafast carrier dynamics in semiconductor nanocrystals. *J. Phys. Chem. B* **104**, 6112–6123 (2000).

- Klimov, V. I., Mikhailovsky, A. A., McBranch, D. W., Leatherdale, C. A. & Bawendi, B. G. Quantization of multiparticle Auger rates in semiconductor quantum dots. *Science* **287**, 1011–1013 (2000).
- Nakamura, S. & Fasol, G. *The Blue Laser Diode: GaN Based Light Emitters and Lasers* (Springer, Berlin Heidelberg, Germany, 1997).
- Wu, L. W. *et al.* Influence of Si-doping on the characteristics of InGaN-GaN multiple quantum-well blue light emitting diodes. *IEEE J. Quantum Electron.* **38**, 446–450 (2002).
- Bidnyk, S. *et al.* High-temperature stimulated emission in optically pumped InGaN/GaN multi-quantum wells. *Appl. Phys. Lett.* **72**, 1623–1625 (1998).

Supplementary Information accompanies the paper on www.nature.com/nature.

Acknowledgements This work was supported by Los Alamos LDRD Funds and the Office of Basic Energy Sciences, Office of Science, US Department of Energy. Sandia National Laboratories is a multiprogram laboratory operated by Sandia Corporation, a Lockheed Martin Company, for the Department of Energy.

Competing interests statement The authors declare that they have no competing financial interests.

Correspondence and requests for materials should be addressed to V.I.K. (klimov@lanl.gov) or M.A. (achermann@lanl.gov).

High levels of atmospheric carbon dioxide necessary for the termination of global glaciation

Raymond T. Pierrehumbert

Department of the Geophysical Sciences, The University of Chicago, 5734 South Ellis Avenue, Chicago, Illinois 60637, USA

The possibility that the Earth suffered episodes of global glaciation as recently as the Neoproterozoic period, between about 900 and 543 million years ago, has been widely discussed^{1–3}. Termination of such 'hard snowball Earth' climate states has been proposed to proceed from accumulation of carbon dioxide in the atmosphere⁴. Many salient aspects of the snowball scenario depend critically on the threshold of atmospheric carbon dioxide concentrations needed to trigger deglaciation^{2,5}. Here I present simulations with a general circulation model, using elevated carbon dioxide levels to estimate this deglaciation threshold. The model simulates several phenomena that are expected to be significant in a 'snowball Earth' scenario, but which have not been considered in previous studies with less sophisticated models, such as a reduction of vertical temperature gradients in winter, a reduction in summer tropopause height, the effect of snow cover and a reduction in cloud greenhouse effects. In my simulations, the system remains far short of deglaciation even at atmospheric carbon dioxide concentrations of 550 times the present levels (0.2 bar of CO₂). I find that at much higher carbon dioxide levels, deglaciation is unlikely unless unknown feedback cycles that are not captured in the model come into effect.

Whereas the problem of initiation of a 'hard snowball' climate state has received detailed attention^{6–8}, most current thinking about deglaciation is based on highly idealized energy balance model (EBM) calculations⁹, which offer an accurate treatment of clear-sky radiation but neglect the seasonal cycle and fix cloud radiative forcing at its present value. Although 0.12 bar of CO₂ is often quoted as a representative deglaciation threshold, a closer reading of the work yields a threshold of 0.29 bar based on Neoproterozoic insolation (Fig. 2 of ref. 9). The same model but with slightly different choices of parameters¹⁰ achieves deglaciation at only 0.16 bar. Because of the weak logarithmic dependence of radiative forcing on CO₂, the EBM results consistently imply that the system should be at least close to deglaciation at 0.2 bar of CO₂.